BACHELOR

A comparison of the Seebeck effect in GIZO and ZnO thin film transistors

Penterman, A.G.J.

Award date:
2013

A Comparison of the Seebeck effect in GIZO and ZnO thin film transistors

Alwin Penterman

Abstract

In this report, the Seebeck effect in zinc oxide and gallium indium zinc oxide thin film transistors has been studied. This is done by measuring the voltage difference between the electrodes of a transistor, which are at a different temperature. The behavior of the Seebeck coefficient vs. the gate voltage and temperature was explained by two different models. The Variable Range Hopping model, which makes use of a model from Vissenberg and Matters (M.C.J.M. Vissenberg, M. Matters, “Theory of the field-effect mobility in amorphous organic transistors”, *Phys. Rev. B*, **57**, 12964, 1998) and the Mobility Edge model, which makes use of a model also used by Horowitz, Hajlaoui and Delannoy (G. Horowitz, R. Hajlaoui, P. Delannoy, "Temperature Dependence of the Field-Effect Mobility of Sexithiophene. Determination of the Density of Traps", *J. Phys. III France*, **5**, 355-371, 1995).

First the I-V curves for a zinc oxide transistor and gallium indium zinc oxide transistor are measured. From these measurements the mobility of these devices is calculated at different temperatures. Using the models to fit these results it is possible to obtain the device parameters of these devices. These device parameters are then used in the models to obtain the theoretical values of the Seebeck coefficient. Next the voltage over the electrodes due to the Seebeck effect is measured for different gate voltages en temperature differences. From these voltages the Seebeck coefficient is calculated, which is then compared to the values calculated using the models.

The theoretical Seebeck coefficients resulting from the VRH model were almost identical to the measured Seebeck coefficients, except for an offset that is still unexplained. Because results from the ME model weren’t as similar to the measurement results, the physical assumptions behind the VRH model are probably closer to the physical reality than those of the ME model. But too few Seebeck coefficient measurement series were made to make sure this result was conclusive.

Contents

Abstract I
Contents II
1 Introduction 1
2 Theory 2
2.1 Seebeck effect 2
2.2 Amorphous semiconductors 4
2.2.1 Density of States 4
2.2.2 Conduction mechanisms 6
2.3 Mobility Edge model 6
2.3.1 Mobility 7
2.3.2 Seebeck coefficient 8
2.4 Variable Range Hopping model 8
2.4.1 Hopping rate 8
2.4.2 Percolation 9
2.4.3 Transport energy 9
2.4.4 Mobility 10
2.4.5 Seebeck coefficient 11
2.5 Field-effect transistor 11
2.5.1 Field-effect 11
2.5.2 Mobility 12
3 Experimental setup and methods 13
3.1 Layout of the samples 13
3.2 Setup 14
3.2.1 Probe station 14
3.2.2 Sample holder 15
3.2.3 Other equipment 15
3.3 Methods 16
3.3.1 Mobility 16
3.3.2 Seebeck Coefficient 17
4 Results 18
4.1 Mobility 18
4.2 Seebeck 20
5 Conclusion and discussion 24
Appendix: Variable Range Hopping model applied to ZnO 25
Bibliography 26

1 Introduction

There is a rapidly increasing interest in electronic devices based on solution processable semiconducting materials. While the research in the area of organic materials has been intensifying, a different class of semiconductors is emerging as an alternative technology. These are the metal-oxide-semiconductors (MOxS).

One of the known MOxS that attracted large interest was zinc oxide (ZnO) because of its nontoxicity, high charge carrier mobility ($\mu \sim 1\ \mathrm{cm^2V^{-1}s^{-1}}$), high transparency to visible light and tunable electrical conductivity. This enables the fabrication of novel devices such as UV light emitting devices and transparent thin-film transistors (TFTs) [1]. Other potential uses are in photo detectors [2], solar cells and light emitting diodes (LEDs) [3]. Furthermore, there are different ways of depositing the ZnO semiconductor, using established industrial techniques such as sputtering [4], dip coating [5], spin coating [6], thermal evaporation [7] and Spray Pyrolysis [8].

Amorphous GIZO is a ZnO-based material of particular interest for the fabrication of high-performance TFTs [9-12] and more interestingly, the prototypes of active-matrix liquid crystal displays [13] and organic light-emitting devices (AMOLEDs) [14-16]. In addition to their transparency GIZO TFTs have unique advantages to allow them to replace polycrystalline silicon (p-Si) TFTs for AMOLEDs. For example GIZO TFTs have a uniform mobility and threshold voltage because of their lack of grain boundaries. Their high charge carrier mobility ($\mu \sim 10\ \mathrm{cm^2V^{-1}s^{-1}}$) and fast transition between on and off states are sufficient to drive large area AMOLEDs. Moreover, it is possible to deposit uniform GIZO thin films over a large area at low temperature by physical vapor deposition techniques, enabling the mass production of AMOLEDs on flexible plastic substrates [9].

In order to learn more about the physical characteristics of both ZnO and GIZO, the Seebeck effect is studied in those materials. The Seebeck effect is the generation of an electromotive force within a (semi)conductor whenever a temperature difference is present. The effect can transform heat into electric energy, or the other way around as a heating or cooling device.

Comparing the measured Seebeck coefficients to the theoretical values that result from various models, provides us with information about the physical characteristics. Even if the models give good fits of the transfer curves, the predicted Seebeck coefficient can still differ from the measurement as the Seebeck coefficient depends on the physical assumptions those the models make.

This report shows that two such models that are typically used for disordered materials, the Mobility Edge (ME) model and the Variable Range Hopping (VRH) model, predict a different Density of States and therefore a different Seebeck coefficient. By comparing the results of those models to the measured values it should be possible to evaluate which model's physical assumptions work better for which material.

2 Theory

In this report the Seebeck effect in the GaInZnO (GIZO) and ZnO field effect transistors is studied and compared to the theoretical values. The Seebeck effect is the generation of an electromotive force within a conductor whenever a temperature difference is present. In order to understand this mechanism, this chapter will start with an explanation of the Seebeck effect, followed by an explanation of amorphous semiconductors and their transport mechanics. After this two models that were derived to approximate these transport mechanics will be treated (the Mobility Edge model and Variable Range Hopping model). These two models are then used to calculate the Seebeck coefficient. Finally the thin film transistor (TFT) will be discussed to give insight in the samples used in the experiments.

2.1 Seebeck effect

The Seebeck effect is a thermoelectric effect which converts a temperature difference directly into a voltage difference. This temperature difference causes charge carriers to diffuse through the material. Because hot charge carriers have more kinetic energy than cold charge carriers, more hot charge carriers diffuse to the cold side than vice versa. Depending on the material, more negative or positive carriers diffuse. Because in the studied materials the diffusion of electrons is dominant, the cold end of the material becomes negatively charged and the hot end positively, resulting in a voltage difference between the two sides. If the dominant diffusing carrier were positive, this voltage difference would also change sign. This electric potential opposes the uneven scattering of carriers, and eventually a steady state is reached where the number of carriers diffusing in one direction is cancelled by the net number of carriers drifting in the opposite direction.

The Seebeck coefficient (sometimes also called thermopower), S, of a material is defined by the magnitude of the induced thermoelectric voltage in response to a temperature difference across the material. If the temperature difference ΔT between the two ends of a material is small, then the Seebeck coefficient of a material is defined as:

$$S = \frac{\Delta V}{\Delta T}, \tag{2.1}$$

where ΔV is the voltage difference over the two ends of the material. [17]

It is also possible to define the Seebeck coefficient from the absolute Peltier coefficient Π. The Peltier coefficient represents how much heat is carried per unit charge through a given material. Since the charge current must be continuous over a junction of two different materials, but the energy of the charge carriers can change due to a different density of states, heat must accumulate or deplete at a junction. The Peltier coefficient is the ratio of the heat current to the charge current at the junction.

$$\Pi = \frac{\dot{Q}}{I} = \frac{\sum_i h_i v_i(x)}{e \sum_i v_i(x)}, \tag{2.2}$$

with h_i the thermal energy of the i th carrier, v_i the velocity of the i th carrier and e the negative elementary charge. [18]

The Seebeck coefficient is related to the absolute Peltier heat by the Thomson relationship

$$\Pi = TS, \tag{2.3}$$

where T is the absolute temperature of the solid. [19]

Assuming that all the involved thermal energy is associated with the charge carriers, the thermal energy can be defined as the difference between the internal energy E_i and the Fermi energy E_F of the charge carriers.

$$h_i = E_i - E_F \tag{2.4}$$

Combining equation (2.2) through (2.4) results in the following equation:

$$S = \frac{1}{eT} \frac{\sum_i h_i v_i(x)}{\sum_i v_i(x)} = \frac{1}{eT} \frac{\sum_i (E_i - E_F) v_i(x)}{\sum_i v_i(x)}. \tag{2.5}$$

When equation (2.5) is changed from a sum over all velocities v_i to a sum over the electron currents $j(E_i) = e v_i$ the following expression arises:

$$S = \frac{1}{eT} \frac{\sum_i (E_i - E_F) j(E_i)}{\sum_i j(E_i)}. \tag{2.6}$$

If the sums are made over a high number of particles, by approximation the following expression can be used:

$$\lim_{n \to \infty} \frac{\sum_i^n f(E_i)}{n} = \int f(E) dE. \tag{2.7}$$

By combining (2.6) and (2.7) the following integral is gained:

$$S = \frac{1}{eT} \frac{\int (E - E_F) j(E) dE}{\int j(E) dE}. \tag{2.8}$$

2.2 Amorphous semiconductors

Semiconductors are materials that conduct by means of thermally activated charge carriers. Because of this the conductivity is zero at absolute zero temperature and rises with temperature. This behavior is informed by the shape of the density of states vs. energy, as explained in the next section.

In crystalline materials, the periodic lattice of the solid forces electrons to be arranged in energy bands neatly separated by regions of energy for which no wavelike electron orbitals exist. A material behaves as a semiconductor if it has a band gap and the nearly free electron model is approximately valid. This is in contrast to metal and semimetals which have no band gap and insulators which have a band gap too large for the nearly free electron model to be valid. (Figure 1) This causes semiconductors to have an electrical conductivity intermediate to that of insulators and metals, and enables the depletion of electrons in a semiconductor. This also enables the easy switching of the current in semiconductors. [20]

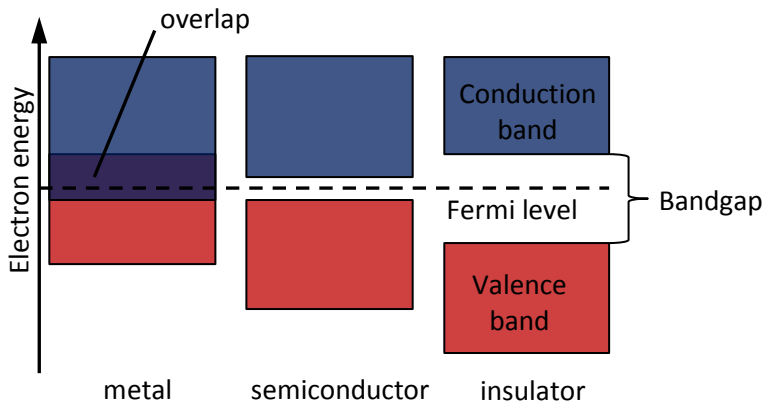

Figure 1: Simplified diagram of the electronic band structure of metals, semiconductors, and insulators.

Because of their properties, semiconductor materials are used in transistors, solar cells, diodes and many more devices which are the foundation of modern electronics. The most common semiconductors are crystalline solids, such as the silicon used in integrated circuits. This report focusses on semiconductors with a different internal structure: amorphous semiconductors. These disordered materials are generally used in thin film structures, in applications which are less demanding of the mobility of the semiconductor.

2.2.1 Density of States

Both electrons and holes are responsible for the conduction in an amorphous semiconductor. The charge carriers may be scattered strongly by the disordered structure, so that the mean free path may sometimes be of the order of the scale of the disorder. Anderson proposed that the states near the band edges are strongly localized (Figure 2). This means that the states are located in a limited area and aren't dispersed through the solid, as with crystalline materials. [20]

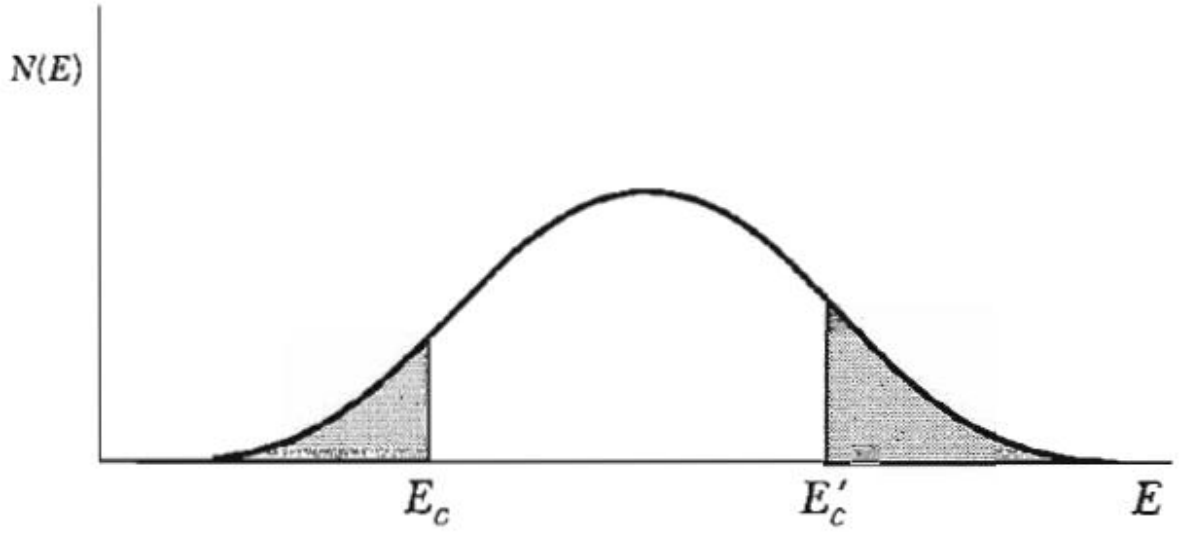

Figure 2: Density of electron states as believed to occur in amorphous solids, when states are non-localized in the center of the band. Localized states are shown shaded. The mobility band edges Ec, Ec' separate the ranges of energy where states are localized and non-localized.

Because the are many localized states, and many of them only differ slightly, they fill a whole spectrum, in contrast to the localized states in crystalline semiconductors, where states usually appear in the form of discrete energy levels, caused by impurity and structural defects. Allowed bands and energy gaps still occur in amorphous semiconductors, because the form of the density of states (DOS) against energy is determined most strongly by local electron bonding configurations. Conduction between these localized states can take place through a thermally assisted hopping process, for which the Hall effect is anomalous and can't be used to find the charge carrier concentration. [20,21]

As seen in Figure 2, the localized states are situated in a band tail. This band tail results from the individual wave functions of the trap states, that fall off exponentially with the distance from their sites. [22] For this report the DOS of trap states is approximated with an exponential density of states:

$$g(E) = \frac{N_0}{k_b T_0} \exp\left(\frac{E}{k_b T_0}\right) \ (-\infty < E \leq 0), \tag{2.9}$$

with N_0 the number of states per volume unit, k_b the Boltzmann constant and k_bT_0 the width of the exponential DOS. Of course this equation only models Andersons density of states for $E < E_C$, but because this is the only part of interest for this report, this isn't a problem. In practice, any DOS can be used as long as *g(E)* increases strongly with *E*. A different example of such density of states is the Gaussian DOS. [24,25]

2.2.2 Conduction mechanisms

Depending on the structure of the material, localized states play two different roles in the conductivity. Either they are traps that prevent the charge carrier transport via extended states. This behavior is probable in a semi-crystalline material. Or the localized states can be used by charge carriers in the so-called hopping transport mode, in which the charge carriers move by thermally activated tunneling between the localized states. This behavior is probable in a completely amorphous material, where there are no extended states because of the disordered structure of the material which limits the path length. [23]

Depending on which of these mechanisms is dominant, the charge transport has to be modeled in a different way. Normally it would be possible to determine which mechanism is dominant by measuring the Hall mobility in a Hall effect experiment. In a magnetic field, there will be no Lorenz force on trapped charges, so a material with many extended states will have a higher mobility. Unfortunately the Hall effect is very difficult to measure experimentally due to the low charge carrier mobilities in the organic semiconductors. Thus it is only possible to determine the dominant mechanism by modeling both mechanisms and checking which model delivers more accurate results. [20,23]

Which role is dominant depends on whether the Fermi energy lies inside or below the band of localized and extended states and further depends on the temperature (Figure 2). The following cases can be distinguished: [23]

a) The Fermi energy lies within the extended states part of the band ($E_c < E_f$). In this case the conductivity will by roughly constant, except at high temperatures, as the extended states are always occupied. This case isn't evaluated in this report, because this looks like the behavior of a crystalline semiconductor.
b) The Fermi energy lies within the trap states part of the band ($E_c > E_f$). This is the case there are two types of conduction possible. At high temperature conduction takes place by the thermal excitation of electrons from the trap states to the extended states, which can be described by the Mobility Edge model (see section 2.3). At low temperatures conduction takes place via hopping between trap states near the Fermi energy, which can be described by the Variable Range Hopping model (see section 2.4).
c) The Fermi energy lies below the band. Here the same two types of conduction are possible as in case b, only a different hopping model is necessary because the hopping doesn't take place around the Fermi energy.

The models used in this report assume that the materials used exhibit conduction of case b.

2.3 Mobility Edge model

Systems where trapping by localized states is the dominant mechanism are often described by the Mobility Edge (ME) model (also called the Multiple Trapping and Release (MTR) model). This model posits that the semiconductor contains both extended and localized states, which are separated at

an energy E_c (see Figure 3), electrons with energies below E_c are trapped and can only move through thermal activation. Electrons with a higher energy inhabit extended states, and thus have a far higher mobility. For this reason the energy E_c is also called the Mobility Edge and the region of energy higher than E_c is called the transport level. Because the Fermi energy E_f lies within the domain of the localized states, and hopping transitions between these states are ignored, all transport has to take place via thermal activation to extended states above the Mobility Edge. The amount of (temporarily) released charge carriers to the extended-state transport level depends on the energy level of the localized states, the temperature and the gate voltage. [22]

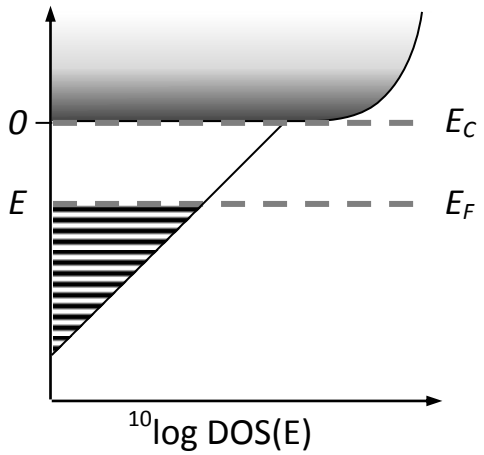

Figure 3: Depiction of the charge distribution and mobility edge assumed in the Mobility Edge model. At energies below the mobility edge Ec states are localized en at energies above Ec states are extended.

2.3.1 Mobility

In the ME model, the conductivity σ is given by the concentration of free carrier n_f times a microscopic mobility μ_0,which is slowly varying with the temperature. [24]

$$\sigma = n_f q \mu_0 \tag{2.10}$$

Here q is the absolute electron charge. Putting $\theta = n_f/n_{tot}$, where $n_{tot} = n_f + n_t$ is the total (free plus trapped) density of charges, (2.10) can be written as

$$\sigma = n_{tot} q \theta \mu_0. \tag{2.11}$$

The relation between the conductivity σ and mobility μ is

$$\sigma = n_{tot} q \mu. \tag{2.12}$$

Combining the previous two equations, the equation of the mobility is as follows,

$$\mu = \frac{\sigma}{n_{tot} q} = \mu_0 \theta. \tag{2.13}$$

The model used for this report, uses a given density of free states N_f, a given density of trapped states N_t and characteristic temperature of the traps T_0 to calculate the local density of states n_f and n_t and thus calculate the mobility. This calculation assumes an exponential Density of States (see section 2.2.1).

2.3.2 Seebeck coefficient

The Seebeck coefficient when the mobility edge allows carrier motion only at energies $E > E_C$ can be obtained from formula (2.8) [26]:

$$S = -\frac{k}{e}\left(\frac{E_C - E_F}{kT} + A_C\right) \text{ for } E_F > E_C \tag{2.14}$$

The term A_C accounts for the fact that the carriers are distributed beyond E_C. The weighted average over the carriers is:

$$A_C = \int_0^\infty \frac{\varepsilon}{kT}\sigma(\epsilon)\mathrm{d}\epsilon \Big/ \int_0^\infty \sigma(\epsilon)\mathrm{d}\epsilon, \tag{2.15}$$

with $\epsilon = E - E_C$. The term A_C remains temperature independent even if the mobility depends on T as long as the dependencies on T and on the integration variable ϵ can be factorized. The function describing the temperature dependence of μ then appears in both the numerator and the denominator and thus cancels. [26]

The values of E_C, E_F and A_C are calculated from the given density of free states N_f, the given density of trapped states N_t and characteristic temperature of the traps T_0.

2.4 Variable Range Hopping model

The Variable Range Hopping (VRH) model describes systems where direct tunneling is responsible for most of the charge transport. In order to use this model, two assumptions have to be made. Firstly, that there is only weak electronic coupling between the single particle sites, so the contribution to the charge transport of the extended states can be ignored. Secondly, that the localized charge carriers hop from an initial site i with energy E_i to a final site j with energy E_j. [27]

2.4.1 Hopping rate

The hopping rate Γ_{ij} is given by the Miller-Abrahams expression:

$$\Gamma_{ij} = \begin{cases} \Gamma_0 \exp\left(-2\alpha R_{ij} - \dfrac{E_j - E_i}{k_b T}\right) & if\ E_j > E_i \\ \Gamma_0 \exp\left(-2\alpha R_{ij}\right) & if\ E_j < E_i \end{cases} \tag{2.16}$$

where Γ_0 is the attempt frequency, α is the inverse of the decay length of the localized wave function, which is taken to be equal for each site, and R_{ij} is the distance between sites. The first

term in the exponent determines the tunnel probability for sites with equal energies and depends on the overlap of the electronic wave functions of sites *i* and *j*. The second term takes the activation energy into account for a hop upwards in energy. For a hop downwards the energy difference between sites is not a restricting factor so it vanishes. [28]

2.4.2 Percolation

The VRH model assumes that the 'optimal' hop would be determined by a trade-off between far hops (large Δx, small ΔE) and short hops (small Δx, large ΔE). The idea behind this is that the conductivity is given by the most difficult hop in a path. If the number of final states for critical hops isn't in the order of unity, the path will die out and will not contribute to charge transport. For a system of dimensionality *d* this argument can be quantified as

$$\Delta x^d \Delta E g_0 = O(1). \tag{2.17}$$

This equation is essentially a percolation argument. To enable conduction in a macroscopic piece of material, an uninterrupted 'percolating' pathway needs to exist between the two contact. In order for such a percolating path to exist, the number of bonds to neighboring sites each site needs to have is of the order of unity.

Because the thermal barrier for hopping to a higher energy state becomes smaller with increasing temperature (2.16), ΔE increases with T, allowing for shorter hops, i.e. Δx decreases with T. For decreasing T the reverse happens. The dependence of the typical hopping distance on temperature is the reason for calling this process 'variable range hopping'. [27]

According to percolation theory [29], the conductivity of the system is given by

$$\sigma = \sigma_0 e^{-s_c} \tag{2.18}$$

where σ_0 is an (unknown) prefactor and s_c is the exponent of the critical percolation conductance $G_c = G_0 e^{-s_c}$. This G_c is determined as follows. Take a reference conductance G and remove all conductances between sites that are lower. For high G, the remaining conductances form isolated clusters. These clusters increase in size with decreasing G. The critical percolation conductance G_c is defined as the value of G where the first infinite cluster is formed. This G_c defines the conductivity (2.18), since it is the most difficult step required for transport through a macroscopic system. [25]

2.4.3 Transport energy

Using the percolation argument it is possible to calculate the typical hop distance R^* and the typical (upward) hop energy E^*. Assuming most hops take place at the Fermi energy E_F (as that is where the most electrons are close to free states) and according to the percolation argument, the relation between R^* and E^* can be obtained from

$$\frac{4}{3}\pi(R^*)^3 \int_{E_F}^{E_F+E^*} g(E)dE = B_c, \tag{2.19}$$

with $B_c \approx 2.8$ the number of bonds per site in a percolating cluster. The typical hop energy electrons are excited to, $E_T \equiv E_f + E^*$, is also called the transport level, as most transport happens via this level. A visual representation of the transport is shown in Figure 4.

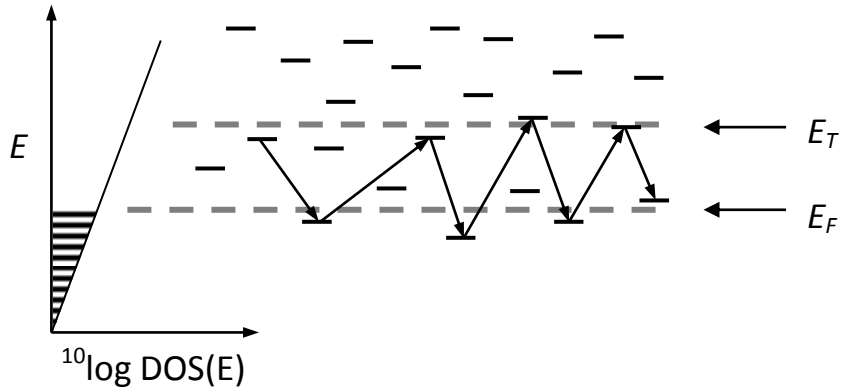

Figure 4: Depiction of hopping transport according to the VRH model. Most charge carriers hop to an energy around transport level E_T because there is a larger number of free states there than at lower energies.

2.4.4 Mobility

One of the two Variable Range Hopping models used in this report is the model studied by Vissenberg and Matters [25]. From equation (2.18) and a differently formulated percolation criterion (related to (2.19)) they obtained the following expression of the conductivity σ:

$$\sigma(\delta, T) = \sigma_0 \left(\frac{\pi N_t \delta (T_0/T)^3}{(2\alpha)^3 B_c \Gamma(1 - T/T_0)\Gamma(1 + T/T_0)} \right)^{T_0/T} \tag{2.20}$$

Vissenberg and Matters use this equation to calculate the current I, which can be inserted in the equation for the field effect mobility that results from the transconductance (2.21). This formula is explained in more detail in section 2.5.

$$\mu_{FE} = \frac{L}{C_i W V_D} \frac{\partial I}{\partial V_G} \tag{2.21}$$

This results in the following formula:

$$\mu_{FE} = \frac{\sigma_0}{e} \left(\frac{\pi (T_0/T)^3}{(2\alpha)^3 B_C \Gamma(1 - T/T_0)\Gamma(1 + T/T_0)} \right)^{T_0/T} \times \left[\frac{(C_i V_G)^2}{2 k_B T_0 \varepsilon_S} \right]^{T_0/T-1} \tag{2.22}$$

The model used for this report uses prefactor σ_0, the localization length of the wavefunction α^{-1}, the characteristic temperature of the trap states T_0 and the total density of localized states N_{loc} as input values to calculate this mobility.

2.4.5 Seebeck coefficient

For unipolar charge carrier transport at a transport level E^* this equation becomes [30]:

$$S = \frac{E^* - E_F}{eT} \tag{2.23}$$

The values of E^* and E_F will have to be calculated using the model to be able to calculate the Seebeck coefficient. To do this the model uses the same input values as the mobility calculation.

2.5 Field-effect transistor

A field-effect transistor (FET) is a transistor where an electric field is used to control the shape and conductivity of a channel of one type of charge carrier in a semiconductor material. The device consists of an active channel through which electrons or holes flow from source to drain. The source and drain terminal conductors are connected to the semiconductor through ohmic contacts. The conductivity of the channel depends on the potential difference between the gate and the source. [31]

The samples used for this report contain thin-film transistors (TFT). Here the semiconductor active layer and metallic contacts are deposited on a substrate consisting of the gate material. A schematic representation can be found in Figure 5. The insulator between the active layer and gate prevents a current between them, because that would negate the voltage difference between source and gate disrupt the current between source and drain.

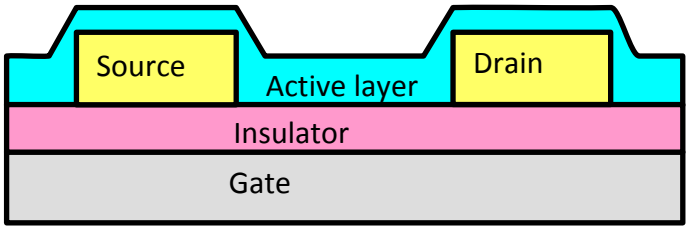

Figure 5: An example of a thin-film transistor (TFT). Most TFTs are deposited on insulating substrates, but in the samples used in this report the substrate is a conductor that also serves as the gate.

2.5.1 Field-effect

A FET operates by means of the field effect. This refers to the altering of the conductivity of a material as The FETs studied in this report are n-channel enhancement-mode devices. In such a device a positive gate-to-source voltage attracts free-floating electrons towards the gate, forming a conductive channel called the accumulation layer. First, enough electrons must be attracted to

counter the depletion region. This phenomenon is called the threshold voltage of the FET. Furthermore this type of device has no natural conductive channel, so applying a positive voltage "switches" it on. [32]

Besides n-type materials, where the main charge carriers are electrons, there also exist p-type materials, where the main charge carries are holes. Furthermore in contrast to enhancement-mode devices, there also exist depletion-mode devices, that have a natural conductive layer that can be closed by applying a voltage difference between the source and gate. [32]

2.5.2 Mobility

There are two conventional ways to estimate the field-effect mobility of field effect transistors. The first is from the saturation current $I_{d,sat}$, equation (2.24) or from the transconductance g_m at low drain current, equation (2.25).

$$I_{d,sat} = \frac{W}{2L}\mu_{FET}C_i\left(V_g - V_0\right)^2 \tag{2.24}$$

$$g_m = \left(\frac{\partial I_d}{\partial V_g}\right)_{V_d \to 0} = \frac{W}{L}\mu_{FET}C_i V_d \tag{2.25}$$

Here, W and L are the channel width and length, respectively; C_i is the insulator capacitance (per unit area) and V_0 the threshold voltage. In this report equation (2.25) is used because it has the advantage of making the measurements at low drain biases, where the accumulation layer is almost uniform over the whole channel. [24]

3 Experimental setup and methods

This chapter is about the experimental setup and methods used in the experiments. First the different samples and their layout are discussed. Next the setup of all the equipment is described, including the connection with the peripherals and the layout of the sample holder. This chapter ends with the methods that were used to calculate the mobility and Seebeck coefficient.

3.1 Layout of the samples

For this report two different types of samples have been used. Both samples consist of a silicon wafer which acts as a gate, with a silicon dioxide (SiO_2) layer of 200 nm deposited on top of it which acts as an insulator. On top of these samples gold was evaporated to form the electrodes. General information about the structures can be found in section 2.5.

The rest of the layout was different between the two types, as can be seen in Figure 6.

Zinc oxide (ZnO) was deposited on the structures of the first sample using spray pyrolysis (at Phillips) while gallium indium zinc oxide (GIZO) was deposited on the structures of the second sample using sputtering (at the Holst Centre). GIZO and ZnO are both transparent disordered materials. The rest of the properties that were used in the models can be found in Table 1.

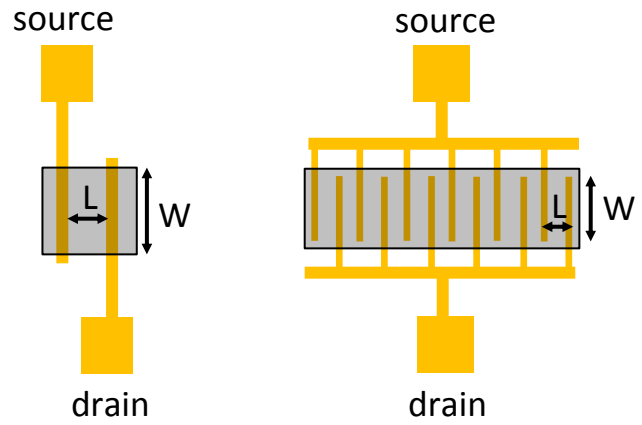

A B

Figure 6: Top views of the two types of structures. The yellow lines represent the electrodes and the grey squares represent the semiconducting material. These structures were deposited on the SiO_2 layer. (A) Structure of the ZnO and GIZO samples used in the Seebeck measurements and the structure of the ZnO sample used in the mobility measurement (B) Structure of the GIZO sample used in the mobility measurement. The width W is a sum over all the individual widths of the electrodes.

Table 1: The properties of the samples that are used in the Mobility Edge and Variable Range hopping models. d_a is the thickness of the accumulation layer. d_g is the thickness of the gate (SiO). ε_R is the relative permittivity of the gate dielectric and C is the capacitance of the gate, calculated using $C = \frac{C}{S} = \frac{\epsilon_R \varepsilon_0}{d}$.

	A (ZnO)	A (GIZO)	B (GIZO)
L (µm)	100	80	10
W (µm)	500	1000	1000
d_a (nm)	1	1	1
d_g (nm)	200	200	200
ε_R (of S_iO)	3.8	3.8	3.8
C (nF/cm^2)	17.0	17.0	17.0

3.2 Setup

The experimental setup used in our experiments is discussed here. The setup can be divided in three parts: the probe station, the sample holder and the peripheral equipment. They are also discussed in that order.

3.2.1 Probe station

The main part of the setup was the Janis probe station (Figure 7), in which the sample and its sample holder (described in 3.2.2) were mounted. The probe station contains 6 probes which are moved by using the arms of the probe station and which could be connected to measuring equipment. In this report probes 3, 5 and 6 were used to contact source, drain and gate ofthe sample, as explained in section 2.5.

The probe station also contains a heating spiral en two temperature sensors that can be used to regulate the sample temperature. To also be able to cool the sample the probe station also contains a cryostat that is connected to a barrel of liquid nitrogen.

Finally the probe station is airtight. To create a vacuum a turbo pump is used. The pressure in the probe station is measured by a pressure meter which was turned off when vacuum was reached, to make sure it didn't influence the measurements.

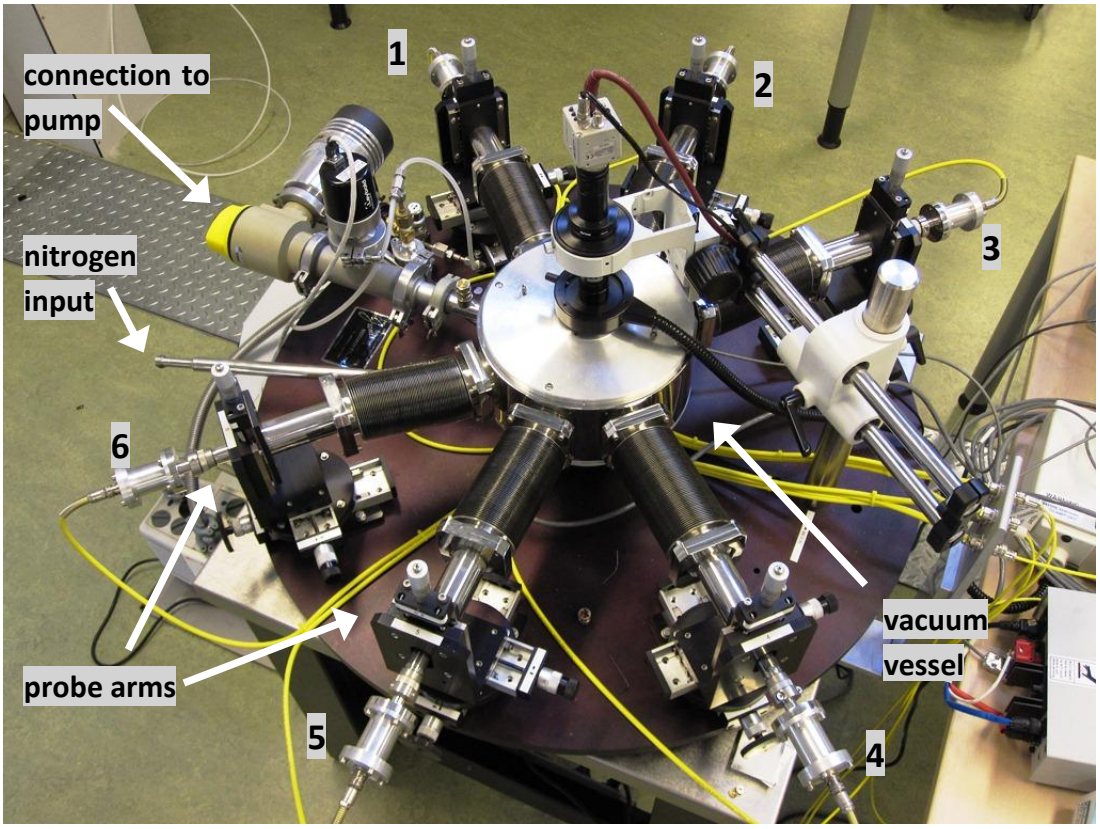

Figure 7: A photograph of the Janis probe station. The numbers indicate the different probe arms.

3.2.2 Sample holder

To be able to mount the samples in the probe station, the sample was placed in a sample holder (Figure 8) which was clamped to the chuck of the probe station. The two Peltier elements beneath the sample were used to heat one end of the sample and cool the other, creating the temperature difference necessary for Seebeck measurements. Apiezon (thermal grease) was added between the sample and the Peltier elements to increase the thermal contact. Because the top of the elements was already electrically insulating, extra insulation wasn't necessary.

Two temperature sensors were fastened between the two screws and the sample, placing them directly above the Peltier elements and thereby also securing the sample. The sensors were separated from the sample by a sheet of Kapton (electrical isolator but good thermal conductor). Because of this setup, it was easy to change and measure the temperature difference over the sample.

The only drawback of the sample holder was that the wafers containing the structures had to be broken down into smaller parts to fit in the holder. Breaking samples had the risk of introducing fractures and thereby ruining the sample.

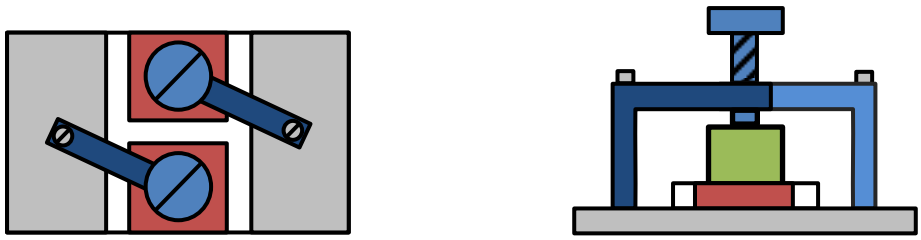

A **B**

Figure 8: A schematic of the sample holder, where A is the top view and B the front view. The sample holder consists of a base plate (gray) that is clamped to the chuck of the probe station. The sample itself is placed on the H-shaped structure (white) and the peltier elements are placed in the space between the arms of that structure (red). The two arms (dark blue) and the screws (blue) serve to secure the sample with the two temperature sensors on top (green).

3.2.3 Other equipment

The outputs of the probes were connected to a Keithley 4200-SCS semiconductor characterization system. This device was used to control and measure the probe voltages and currents and store the results of our measurements.

The wiring of the heating equipment and temperature sensors inside the probe station connect to the outside through an insulated duct. Here these cables were connected to a number of peripherals:

The heating spiral of the probe station was controlled by a Scientific Instruments model 9700, that also received the output of the probe station's two temperature sensors. This allowed this controller to maintain a stable temperature.

The two Peltier elements were connected to two power supplies by Delta Elektronika. These power supplies were controlled by hand to create the necessary temperature difference. This temperature difference was then measured by a Scientific Instruments model 9302, that was connected to the two temperature sensors on the sample.

3.3 Methods

To be able to compare the theoretical and experimental values of the Seebeck Coefficient, two types of measurements had to be done. The two types of measurement series were necessary to determine the relation of respectively the mobility μ and Seebeck coefficient S to both the gate voltage V_g and temperature T. The theoretical relation between the mobility and the Seebeck coefficient is shown in sections 2.3.2 and 2.4.5. This section focusses on the methods by which these measurements were taken.

3.3.1 Mobility

To calculate the mobility, first a gate voltage sweep was made. To be able to do this, first part of the insulator layer had to be scratched away, so that it was possible to contact an electrode to the gate. Two other electrodes were connected to the two contact pads of the structure, which were used as source and drain (see Figure 6). After this the following voltages were applied: V_{source} = 0V and V_{drain} = 2V. The drain current I_{drain} was measured while the gate voltage V_{gate} was swept over a certain domain. The results of this measurement were used to calculate the mobility of the transistor, using an equation derived from equation (2.25):

$$\mu_{FET} = \left(\frac{\partial I_{drain}}{\partial V_{gate}}\right)_{V_{drain}\to 0} \frac{L}{W V_{drain} C_i} \tag{3.1}$$

Here, W and L are the channel width and length, respectively; C_i is the insulator capacitance (per unit area). [24]

After a few measurement series at the same temperature, the temperature was changed using the cryostat and heating spiral. Before changing the temperature the probes were removed from the sample to avoid damaging it. After the temperature became stable, the connectors of the probes were connected to each other and the ground, before replacing them on the sample, to make sure there were no excess voltages within the system. After removing interconnection and reconnecting the equipment, measurements were resumed.

Because the threshold voltage V_T (see section 2.5.1) varied between measurement series, the mobility results were shifted along the voltage axis such that the transistor always switched on at

0V. This was necessary to be able to compare the results. The $V_{threshold}$ of a measurement series was assumed to be at the voltage where I_{drain} was between 10e-12A and 100e-12A.

The Mobility Edge model (section 2.3) and Variable Range Hopping model (section 2.4) were then used to fit these mobility measurements, by changing the parameters until the theoretical and experimental results had the smallest possible difference. Because the versions of these two models that were used for this report were made for p-type materials and the samples were n-type, the gate voltages had to be taken negative in the model to be able to analyze the results.

3.3.2 Seebeck Coefficient

To calculate the Seebeck coefficient of the sample at a certain gate bias V_G and certain sample temperature T, drain voltage sweeps had to be made at V_S = 0V under various temperature differences ΔT between sources and drain (including ΔT = 0K).

During the sweep of the drain voltage V_D, the source current I_S and drain current I_D were measured. At the V_D where $I_S = I_D$, the applied voltage difference $V_{SD} = V_S - V_D$ negates the voltage difference caused by the Seebeck effect ΔV, so there $\Delta V = -V_{SD} = V_D$ (see Figure 9).

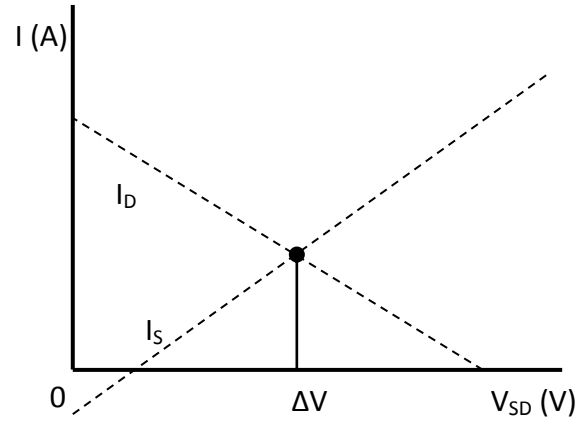

Figure 10: A schematic representation of a graph wherein ΔV is found at the intersection of I_D and I_S.

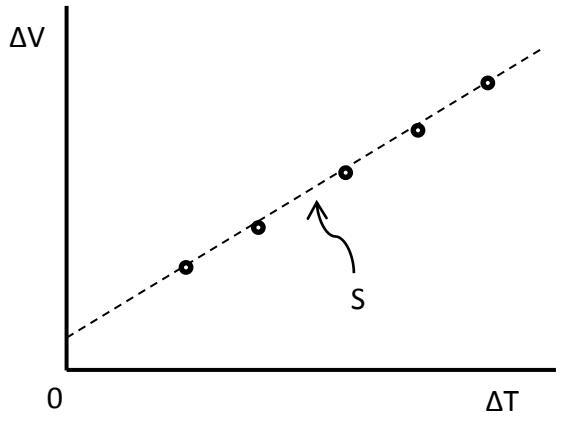

Figure 9: A schematic representation of a graph wherein S is found by taking the slope of the fit of ΔV against ΔT.

By varying the temperature difference between measurements, the ΔV was found for various ΔT, at a constant T and V_G. To accurately measure the temperature differences, one temperature measurement was made at the start of the sweep, on when the currents were the same and a final one at the end of the sweep. The Seebeck coefficient S was then found using the following formula (see Figure 10):

$$S = \frac{\Delta V}{\Delta T} \tag{3.2}$$

This way the Seebeck coefficient was calculated for different sample temperatures and gate biases.

4 Results

In this chapter the Seebeck measurements on zinc oxide (ZnO) and gallium indium zinc oxide (GIZO) are compared to the Seebeck coefficients predicted on basis of the fits to the transfer curves and equations (2.14) and (2.23). The method by which this is done is discussed in more detail in section 2.3.2.

The theoretical Seebeck coefficients are calculated from the density of states parameters that are obtained after fitting the mobility in transfer curves at different temperatures. This will be done for both the Mobility Edge (ME) model and the Variable Range Hopping (VRH) model that are discussed in section and 2.3 and 2.4 respectively. This method is discussed in more detail in section 3.3.1.

This chapter starts with the analysis of the mobility results. After this the results for the Seebeck coefficient are analyzed.

4.1 Mobility

In this section the mobility of the materials will be analyzed and compared to the predictions. In is important to note that different implementations of the Variable Range Hopping model were used for both materials. The preferred model had problems fitting the mobility of zinc oxide, as can be seen in the appendix. The further differences between the models should be minimal, because they are based on the same equations.

The first material to be analyzed is zinc oxide (ZnO). A comparison of the mobility calculations and measurements shows that the ME model mobility fit was more accurate around 300K than the VRH mobility fit (Figure 12 and Figure 13). The VRH model mobility fit has a better overall result, because while the predictions around 300K are almost the same as those of the ME model, the predictions around 150K are closer to the measurements. To find a beter solution for the ME model at lower temperatures, another set of parameters is used (Figure 11). Only this set doesn't have much use, as it isn't accurate at the higher temperatures.

The spread in the found density of state parameters for both models (Table 2 and Table 3) was this large because it was impossible to fit the mobility measurements of the ZnO material across the whole temperature spectrum. It was only possible to fit the mobility measurements across approximately a 30 K range of temperatures (Figure 11 and Figure 12), so the values were recorded for a fit around 200 K and one around 300 K. This means that the used relation between the temperature and mobility is probably incorrect, possibly because its density of states isn't exponential, contrary to the assumption.

For the ZnO material, the VRH model was more accurate overall (Figure 12) and the ME model was more accurate around 300 K (Figure 13) at the expense of accuracy at other temperatures.

Table 2: The DOS parameters resulting from fitting the ME model results to the measured mobility values of ZnO at different temperatures.

fit temperature (K)	μ_0 (cm^2/Vs)	N_{trap} ($1/m^3$)	N_{free} ($1/m^3$)	T_0 (K)
150	2,0	0,20e26	0,20e26	650
300	47,0	0,45e26	0,45e26	990

Table 3: The DOS parameters resulting from fitting the VM model results to the measured mobility values of ZnO at different temperatures.

fit temperature (K)	T_0 (K)	σ_0 (S/m)	α^{-1} (m)
200	520	1,98e6	1,00e-9
300	670	2,11e7	8,40e-10

Table 4: The DOS parameters resulting from fitting the ME model results to the measured mobility values of GIZO at different temperatures.

fit temperature (K)	μ_0 (cm^2/Vs)	N_{trap} ($1/m^3$)	N_{free} ($1/m^3$)	T_0 (K)
250	32,0	0,50e26	0,50e26	390
300	32,0	0,42e26	0,42e26	390

Table 5: The DOS parameters resulting from fitting the VRH model results to the measured mobility values of GIZO at different temperatures.

fit temperature (K)	T_0 (K)	σ_0 (S/m)	α^{-1} (m)
250	450	7,4e10	8,57-10
300	540	4,6e10	10,5e-10

The second material to be analyzed is gallium-indium-zinc-oxide (GIZO). A comparison of the mobility calculations and measurements showed that the ME model produced more accurate mobility results overall for this material. Because the theoretical results were relatively accurate at all temperatures and because of time constraints, the parameters weren't changed a second time to fit the measurements at another temperature, as was done with the ZnO sample. The results displayed in Figure 14 and Figure 15 are of the second sample, measured at 300 K.

Fitting the mobility of the GIZO material was easier than fitting the ZnO mobility. Where it was impossible to find ZnO parameters that produce an accurate prediction over the whole temperature spectrum, it was possible for GIZO (Figure 15). This means that the relation between temperature and mobility of the GIZO material corresponds to that of the models.

For the GIZO material, the ME model was the most accurate over the temperature domain (Figure 14), as it was impossible to make both the upper lines convex and the lower lines concave for the VRH model (Figure 15). Why the model behaves this way is still inconclusive.

4.2 Seebeck

In this section the Seebeck coefficient of the materials will be analyzed and compared to the predictions.

Because measurements of the Seebeck coefficient of ZnO and GIZO were made only at a temperature of 300 K, the results were compared only for that temperature (Figure 16 and Figure 17). More measurements were planned, but were not performed because of time limitations.

In the analysis of GIZO two samples were used. On the first sample mobility measurements were performed at a temperature of 250 K. This sample shorted out during the measurements of the Seebeck coefficient, so there weren’t any Seebeck coefficient results for this sample. Further measurements were performed on another GIZO sample.

For both materials, a comparison of the calculations and the measurements showed that the shape of the measurement graph was similar to the shape of the VM model graph, but unlike that of the ME model graph. The slope of the ME model graph is greater than the slope of the measured values. This means that the transport energy level doesn't increase as fast with the gate voltage as the ME model predicts.

During the comparison it was also noticed that for both materials, the results for both models are each other's translation along the y-axis, despite resulting from different parameters. For ZnO this could mean that at a higher temperature there is a fixed number of extra available charge carriers that moves under influence of the thermo-electric effect. Because Seebeck coefficient measurements were only made for one temperature, it isn’t possible to determine which at which temperature the theoretical results are the most accurate. This explanation does not hold for GIZO, as both measurements were done on different samples at the same temperature. It could be that

because of a difference in structure there is a fixed amount of extra free charge carries, but this hasn't been tested yet.

Next the theoretical Seebeck coefficients of the two materials were compared. The maximum difference between the different theoretical results for the GIZO material was 100 µV/K (Figure 17) while the maximum difference between the different theoretical results for the ZnO material was more than 200 µV/K (Figure 16). The shapes of the different theoretical results versus the gate bias also had a more similar shape for the GIZO material than for the ZnO material, but the GIZO material results did have a larger offset compared to the measurements.

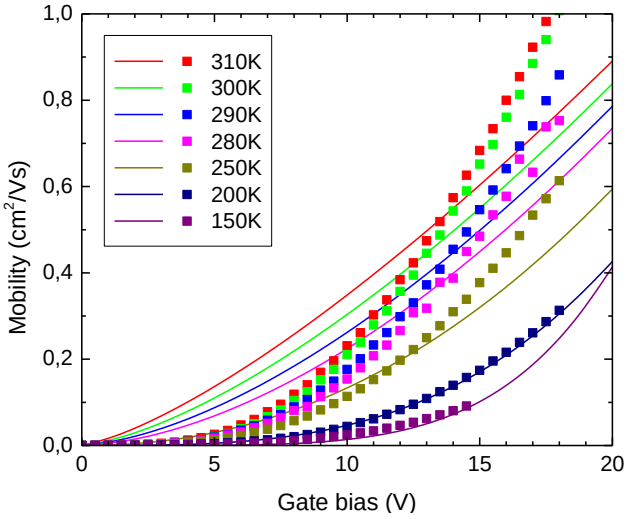

Figure 11: Comparison of the measured mobility and the theoretical mobility as calculated by the VRH model at different temperatures of the ZnO sample. Squares represent measurements, lines represent model results. The model parameters were chosen such that the model results approximate the measured values around 200 K.

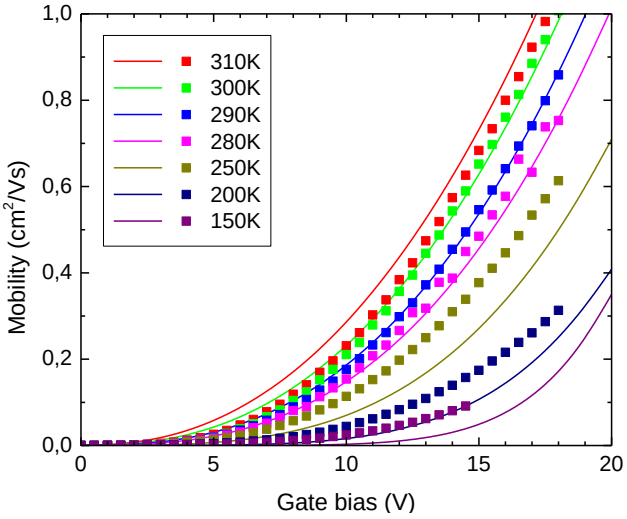

Figure 12: Comparison of the measured mobility and the theoretical mobility as calculated by the VRH model at different temperatures of the ZnO sample. The squares represent measurements, the lines represent model results. The model parameters were chosen such that the model results approximate the measured values around 300 K.

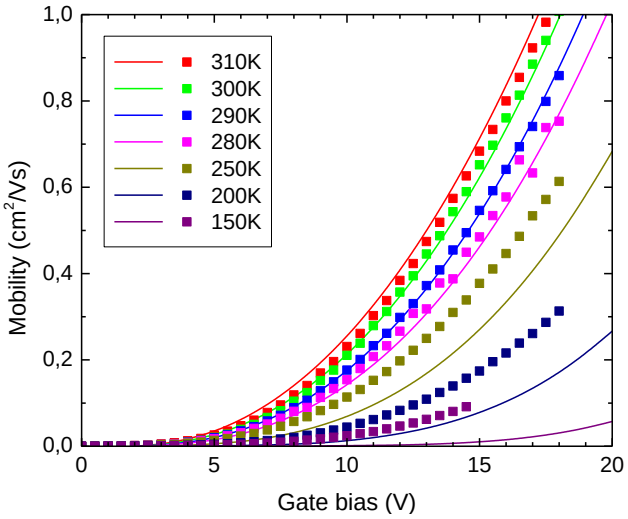

Figure 13: Comparison of the measured mobility and the theoretical mobility as calculated by the ME model at different temperatures of the ZnO sample. The squares represent measurements, the lines represent model results. The model parameters were chosen such that the model results approximate the measured values around 300 K.

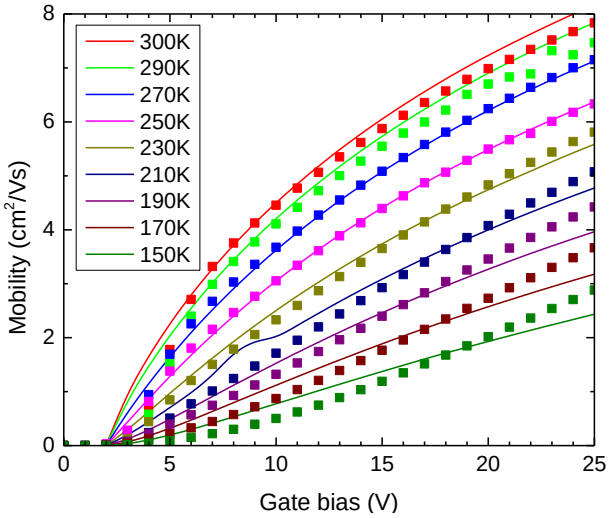

Figure 14: Comparison of the measured mobility and the theoretical mobility as calculated by the ME model at different temperatures of the GIZO sample. The squares represent measurements, the lines represent model results.

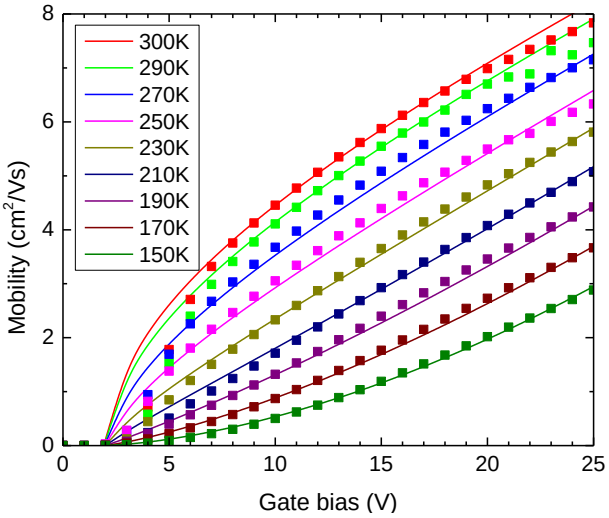

Figure 15: Comparison of the measured mobility and the theoretical mobility as calculated by the VRH model at different temperatures of the GIZO sample. The squares represent measurements, the lines represent model results.

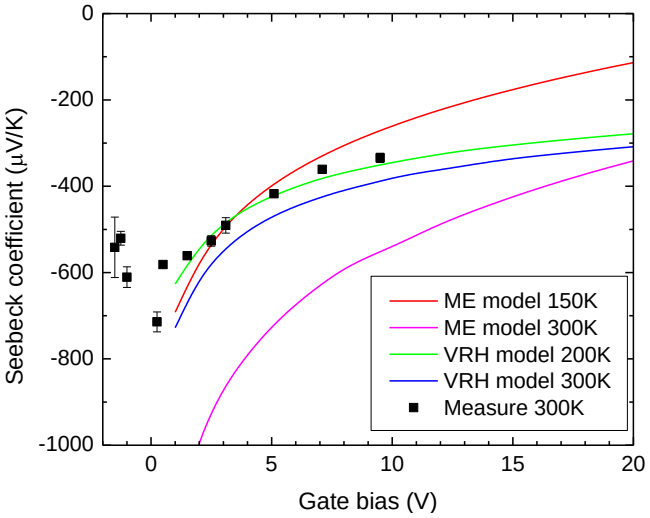

Figure 16: Comparison of the calculations of the Seebeck coefficient and the measurements of the Seebeck coefficient at 300 K of the ZnO sample. The 300K model lines resulted from the parameters found in a mobility fit at 300 K. The others lines resulted from mobility fits at different temperatures.

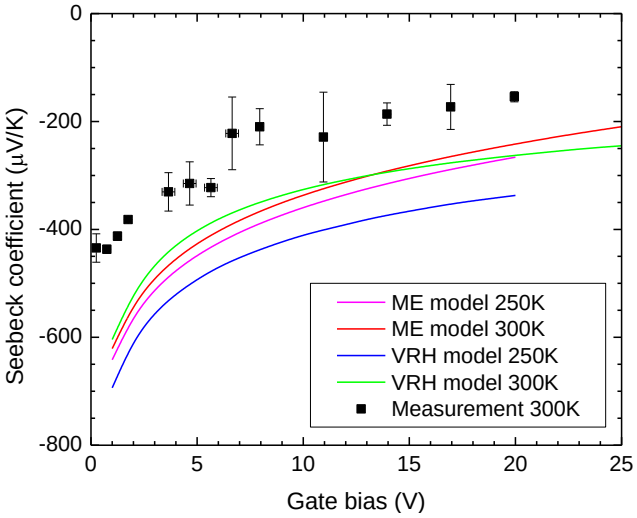

Figure 17: Comparison of the calculations of the Seebeck coefficient and the measurements of the Seebeck coefficient at 300 K of the GIZO samples. The 300K model lines resulted from the parameters found in a mobility fit at 300K. The others lines resulted from mobility fits at different temperatures.

5 Conclusion and discussion

In this report the Seebeck effect is studied in zinc oxide (ZnO) and gallium indium zinc oxide (GIZO) thin film transistors. The theoretical results of the Mobility Edge (ME) model and Variable Range Hopping (VRH) model were compared to the measurements to be able to tell something about the physical properties of the materials.

In the last chapter it was shown that the VRH model results were almost identical to the measurements, except for an offset in the Seebeck coefficient, for which the reason still isn't clear. This offset was 50 µV/K for ZnO and 100 µV/K for GIZO. Still, because the shape of the theoretical ME result wasn't as similar to the measurement results as the shape of the theoretical VRH result, the physical assumptions behind the VRH model are probably closer to reality than those behind the ME model.

The Density of States parameters of the ME model had a far smaller spread for the GIZO material than for the ZnO material. The difference between the results of the VRH model weren't as evident, but the maximum difference of the GIZO material parameters was still smaller. The above results could indicate that the density of states of the GIZO material was closer to the theoretical DOS used by both models than the density of ZnO material, but there weren't enough results to prove this conclusively.

Furthermore the reason the ZnO didn't behave was probably that it had more disorder. This follows from μ (ZnO) < μ (GIZO) and S (ZnO) > S (GIZO), which causes a broader Density of States than the exponential one that was used here. Another parameter that shows is T_0 as T_0 (ZnO) > T_0 (GIZO), which means that the trap states are deeper.

Because only a few Seebeck measurement series were done for this report, and only around room temperature there is a probability that the results aren't general. In order to be completely sure about this conclusion, more measurements will have to be done.

Appendix: Variable Range Hopping model applied to ZnO

Originally the same VRH model was for the ZnO material as for the GIZO material. The density of states parameters were found by fitting the transfer curves (Figure 18 and Table 6). These same parameters were used to calculate the theoretical Seebeck coefficient (Figure 19). Unfortunately it was impossible to gain a smooth graph of the theoretical Seebeck coefficient using these parameters. This could be because the T_0 value is outside of the realistic domain for this material, but this is not certain.

Because of this a different implementation of the Vissenberg-Matters model was used instead. This was possible because both models use the same density of state parameters, allowing the original model to calculate the theoretical Seebeck coefficient as the new model wasn't able to. The results are discussed in section 4.1.

Table 6: The DOS parameters resulting from fitting the VRH model results to the measured mobility values of ZnO.

fit temperature (K)	T_0 (K)	σ_0 (S/m)	α^{-1} (m)
300	3100	140e10	9,5e-10

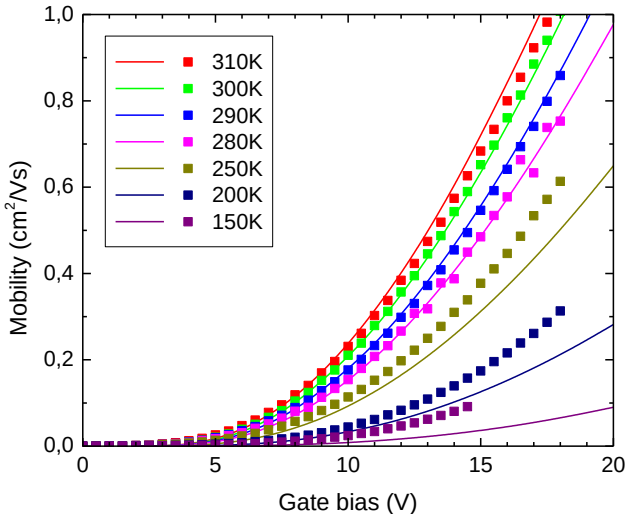

Figure 18: Comparison of the measured mobility and the VRH model results of the ZnO material at different temperatures. Squares represent measurements, lines represent model results. The model parameters were chosen so that the model results approximate the measured values around 300K.

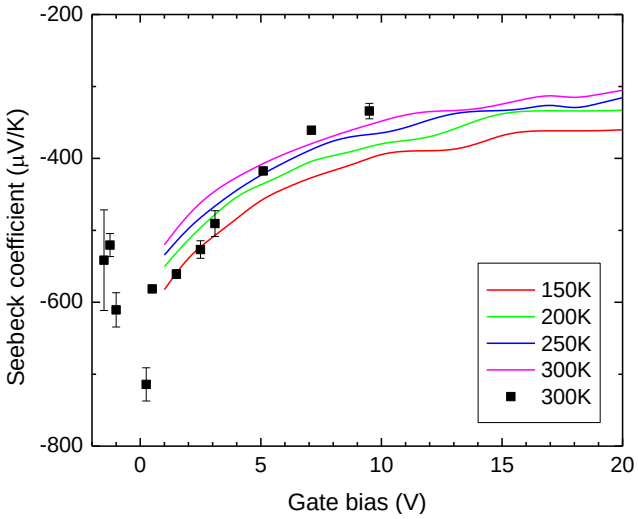

Figure 19: Comparison of the calculations of the theoretical Seebeck coefficient at different temperatures and Seebeck coefficient measurements at 300K for the ZnO sample. The squares represent the measurements, and the lines the theoretical results.

Bibliography

[1] H. Hosono, *J. Non-Cryst. Solids*, **352**, pp. 851, 2006

[2] Y. Liu, C.R. Gorla, S. Liang, N. Emanetoglu, Y. Lu, H. Shen, M. Wraback, *J. Electron. Mater.*, **29**, pp. 60, 2000

[3] W.J. Jeong, S.K. Kim, G.C.Park, *Thin Solid Films*, **506–507**, pp. 180, 2006

[4] P.F. Carcia, R.S. McLean, M.H. Reilly G. Nunes, "Transparent ZnO thin-film transistor fabricated by rf magnetron sputtering", *Appl. Phys. Lett.*, **vol. 82**, **no. 7**, pp. 1117–1119, 2003

[5] Y. Ohya, T. Niwa, T. Ban, Y. Takahashi, "Thin film transistor of ZnO fabricated by chemical solution deposition", *Jpn. J. Appl. Phys.*, **vol. 40**, **no. 1**, pp. 297–298, 2001

[6] Y.J. Chang, D.H. Lee, G.S. Herman, C.H. Chang, "Highperformance, spin-coated zinc tin oxide thin-film transistors", *Electrochem. Solid-State Lett.*, **vol. 10**, **no. 5**, pp. H135–H138, 2007

[7] O.A. Fouad, A.A. Ismail, Z.I. Zaki, Z.M. Mohamed, "Zinc oxide thin films prepared by thermal evaporation deposition and its photocatalytic activity", *Appl. Catal. B: Environ.*, **vol. 62**, **no. 1/2**, pp. 144–149, 2006

[8] T. Prasada Rao M.C. Santhoshkumar, "Highly oriented (1 0 0) ZnO thin films by spray pyrolysis", *Appl. Surf. Sci.*, **vol. 255**, **no. 16**, pp. 7212–7215, 2009

[9] K. Nomura, H. Ohta, A. Takagi, T. Kamiya, M. Hirano, H. Hosono, *Nature (London)*, **432**, pp. 488, 2004

[10] H. Yabuta, M. Sano, K. Abe, T. Aiba, T. Den, H. Kumomi, K. Nomura, T. Kamiya, H. Hosono, *Appl. Phys. Lett.*, **89**, 112123,2006

[11] D. Kang, H. Lim, C. Kim, I. Song, J. Park, Y. Park, J. Chung, *Appl. Phys. Lett.*, **90**, 192101, 2007

[12] M. Kim, J.H. Jeong, H.J. Lee, T.K. Ahn, H.S. Shin, J.S. Park, J.K. Jeong, Y.G. Mo, H.D. Kim, *Appl. Phys. Lett.*, **90**, 212114, 2007

[13] T. Hirao, M. Furuta, H. Furuta, T. Matsuda, T. Hiramatsu, H. Hokari, M. Yoshida, *in Proceedings of SID Digest*, **37**, pp. 18, 2006

[14] H.N. Lee, J.W. Kyung, S.K. Kang, D.Y. Kim, M.C. Sung, S.J. Kim, C.N. Kim, H.G. Kim, S.T. Kim, *in Proceedings of IDW*, pp. 663–666,2007

[15] S.K. Park, C.S. Hwang, J.I. Lee, S.M. Chung, Y.S. Yang, L.M. Do, H.Y. Chu*, in Proceedings of SID Digest*, **13**, pp. 25,2006

[16] J.K. Jeong, M.Kim, J.H. Jeong, H.J. Lee, T.K. Ahn, H.S. Shin, K.Y. Kang, H. Seo, J.S. Park, H. Yang, et al., *in Proceedings of IMID*, pp. 145–148,2007

[17] P.L. Taylor, “Seebeck Coefficient at the Curie Temperature: Specific Heat of Charge Carriers in Ferromagnets”, *Phys. Rev. B*, **7**, pp. 1197-1198, 1973

[18] M.A.Laughton, D.F. Warne, "Electrical Engineer's reference book", Oxford: George Newnes Ltd, 2003

[19] L.I. Anatychuk, O.J. Luste, "Generalized thermoelectric Thomson relations", *Thermoelectrics, 2003 Twenty-Second International Conference on - ICT*, pp. 491-492, 2003

[20] C. Kittel, “Introduction to Solid State Physics”, New York: Wiley, 2005

[21] S. Barovski, “Charge Transport in Disordered Solids with Applications in Electronics”, England: John Wiley & Sons Ltd, 2006

[22] J.D. Joannopoulos, G. Lucovsky, “The Physics of Hydrogenated Amorphous Silicon II”, Berlin Heidelberg: Springer-Verlag, 1984

[23] E.J. Meijer, “Charge transport in disordered organic field-effect transistors”, Ph.D. thesis, Delft University of Technology, 2003

[24] G. Horrowitz, R.Hajlaoui, P. Delannoy, "Temperature Dependence of the Field-Effect Mobility of Sexithiophene", *J. Phys. III France*, **5**, 355-371, 1995

[25] M.C.J.M. Vissenberg, M. Matters, “Theory of the field-effect mobility in amorphous organic transistors”*, Phys. Rev. B*, **57**, 12964, 1998

[26] H. Fritzsche, “A general expression for thermoelectric power”, *Solid State Communications*, **9**, pp. 1813-1815, 1971

[27] M. Kemerink, “Organic electronics lecture 4”, Eindhoven University of Technology, 2009

[28] R. Coehoorn, W.F. Pasveer, P.A. Bobbert and M.A.J. Michels, “Charge-carrier concentration dependence of the hopping mobility in organic materials with Gaussian disorder”*, Phys. Rev. B*, **72**, 155206, 2005

[29] M. Sahimi, "Applications of Percolation Theory", Taylor & Francis, London, 1994

[30] B. Maennig, M. Pfeiffer, A. Nollau, X. Zhou, K. Leo, P. Simon, "Controlled p-type doping of polycrystalline and amorphous organic layers: Self-consistent description of conductivity and field-effect mobility by a microscopic percolation model", *Phys. Rev. B*, **64**, 195208, 2001

[31] J. Millman, C. Halkias, "Electronic devices and circuits", Singapore: McGraw-Hill international book company, 1985

[32] N.R. Malik, "Electronic circuits: analysis, simulation, and design", Englewood Cliffs, NJ: Prentice Hall, 1995